High-Temperature Mechanical Behavior and Hot Rolling of AA705X

S.F. HARNISH, H.A. PADILLA, B.E. GORE, J.A. DANTZIG, A.J. BEAUDOIN, I.M. ROBERTSON, and H. WEILAND

High-temperature mechanical behavior and processing performance of 705X aluminum alloys is examined, employing a combination of mechanical testing, microscopy, and computational modeling. We perform hot uniaxial compression tests over a range of temperatures and strain rates and fit the data to power-law constitutive models. These models are supported and expanded by microscopy and calorimetry, which help to elucidate the operating deformation mechanisms and examine damage evolution. The mechanical behavior constitutive relations are implemented in a finite-element code to simulate the hot rolling process. The results of the rolling simulation are used to predict final product crystallographic texture, which is compared with experimental electron backscattered diffraction measurements for model validation. Finally, we propose a parameter to characterize the development of damage during processing. This work provides a solid foundation for the design of thermomechanical processing of these alloys to maximize yield and optimize process performance.

I. INTRODUCTION

HIGHLY alloyed aluminum has been one of the most widely successful and broadly applicable materials developed for engineering structures in the last century. Industries that have benefited from the development of these alloys include packaging, automotive, and aerospace. The Al-Zn-Mg-Cu 7000 series alloys have seen extensive use in the aerospace industry. The 705X alloys, which exhibit both a high fracture toughness and high resistance to stress corrosion cracking when brought to a T7 temper, were specifically developed to be used in plate form for structural wing components in commercial aircraft.[1]

Fabrication of these products begins with direct chill casting followed by heat treatment for homogenization. The slabs are then taken from the solution treatment furnace, and hot rolled through several passes until the desired final thickness is achieved. The rolled material is then quenched and stretched. In the final step, the plate is aged to precipitate the strengthening phases. The thermomechanical history in these processes produces through-thickness gradients in constituent phase, and precipitate distributions, texture, and grain structure, which all lead to gradients in mechanical properties. A detailed review and study of the relationship between microstructure, strength, and toughness in aged 7050 plate, with consideration of anisotropy, has been given by Dumont *et al*.[2] It is desirable to look further upstream and define the thermomechanical processing window (TPW), *i.e*., the range of physically realizable processing parameters (roll speed, lay-on temperature, reduction, lubricant properties, *etc*.) that lead to production of a quality product.

To gain a better understanding of the limits of the TPW and what microstructural processes govern the material behavior near those limits, experiments and numerical simulations have been performed. Material characterization studies under different temperature and stress histories provide an understanding of the precipitate and second-phase structure, and indicate active deformation mechanisms. Guided by these results, and industrial practice, a homogenization procedure is developed and used to prepare samples for mechanical testing. A novel test procedure is also introduced, which permits identifying the onset of damage. The mechanical test data are then used to develop constitutive relations appropriate for hot rolling. We pose a rolling model through introduction of the constitutive relations into established procedures for finite element analysis of viscoplastic flow, with subsequent post-processing of material history along streamlines to predict evolution of crystallographic texture in the final product. A contribution of this modeling effort lies in the tuning of boundary conditions for friction so as to establish agreement between measured and predicted gradients in crystallographic texture. To complete the structure-properties-processing triangle, we interpret simulation results on the basis of the experimental conditions associated with damage initiation.

II. MATERIAL CHARACTERIZATION

In order to understand the mechanical behavior of AA 705X under hot rolling conditions, it is essential to identify the phases present as a function of various thermal histories. To this end, the microstructure of hot-rolled 7055 was examined in the as-received state (T79), after a heat treatment in which sections of the plate were first homogenized at 480 °C for 1 hour, then held at temperatures of 500 °C, 460 °C, or 420 °C for 3 minutes, and then quenched. Transmission electron microscopy samples were prepared using conventional techniques, and were then examined in a JEOL* 4000 at an operation voltage of 300 keV.

S.F. HARNISH, formerly with the Department of Mechanical and Industrial Engineering, University of Illinois, is with Gamma Technologies, Inc., Westmont, IL. H.A. PADILLA, J.A. DANTZIG, and A.J. BEAUDOIN are with the Department of Mechanical and Industrial Engineering, University of Illinois, Urbana, IL 61801. B.E. GORE and I.M. ROBERTSON are with the Department of Materials Science and Engineering, University of Illinois. H. WEILAND is with the Alcoa Technical Center, Alcoa, PA 15069.

Manuscript submitted May 20, 2004.

*JEOL is a trademark of Japan Electron Optics Ltd., Tokyo.

The as-received microstructure, shown in Figure 1(a), consisted of elongated particles of the strengthening η-phase ($MgZn_2$) throughout the matrix and along the grain boundaries, with smaller particles of η^0 strengthening phase in the matrix. In addition, coherent Al_3Zr precipitates (20 to 50 nm), which hinder recrystallization, are distributed throughout the matrix.[3] While the Al_3Zr precipitates are stable at high temperature due to their high melting point (~1500 °C), the η-type particles can be put back into solution *via* heat treatment at 480 °C. An example of such a homogenized microstructure is shown in Figure 1(b); here, the sample has been solutionized, and then quenched after a 3-minute hold at 500 °C. As would be expected, the microstructure is free of all precipitates and contains only Al_3Zr precipitates. The helical dislocations in this image are a result of a climb-assisted process due to the supersaturation of vacancies retained during the quench from high temperatures. Figures 1(c) and (d) show microstructures obtained after first cooling to, and then quenching from, 460 °C and 420 °C, respectively. In Figure 1(c), the microstructure is still free of η-type particles; however, large constituent phases (such as Al_7Cu_2Fe) have formed and, as shown, interact with the dislocations at subgrain boundaries. This dislocation structure suggests that this sub-grain boundary was mobile at the homogenization temperature.[4] As the holding temperature is lowered further, η particles begin to reprecipitate, nucleating preferentially at dislocations and on Al_3Zr particles. As an example, the arrow in Figure 1(d) highlights η particles nucleating on the dislocations in a grain boundary. These results correlate well with differential scanning calorimetry analysis. A temperature of 480 °C is sufficient to dissolve the strengthening phases. This provides a basis for the homogenization procedure employed in mechanical testing, to be described subsequently. Although an example is not shown here, cooling to lower temperatures (=380 °C) increases the number and size of the η particles.

Insight into the thermomechanical processing history of the as-received material can be gained from examination of texture gradients through the plate thickness. Roll gap geometry in plate rolling, combined with frictional effects induced by the work rolls, promotes a nonuniform deformation field. Away from the center plane, shear deformations are developed as a consequence of boundary conditions.[5] Studies of rolling with high reduction ratio show the 45-deg normal direction (ND)–rotated cube, $\{001\}\langle 110\rangle$, as a dominant component of the texture in regions of high shear.[6] Combined experiment and finite-element simulation have shown the position of maximum shear texture development to lie 80 pct of the distance from the centerline to the surface.[7] Such gradients in texture have been observed in 7010 plate, with the centerline bearing components typical of plane strain compression and, closer to the surface, a transition to a texture with $\{001\}\langle 110\rangle$ as the dominant component.[8]

Slices preserving the ND were taken from 25-mm-thick plate, and experimental texture measurements were made on the top, middle ($t/2$), bottom, and quarter-thickness planes ($t/4$ and $3t/4$). The surface of each plane was polished with 3-μm alumina slurry and electroetched in a solution of 25 pct

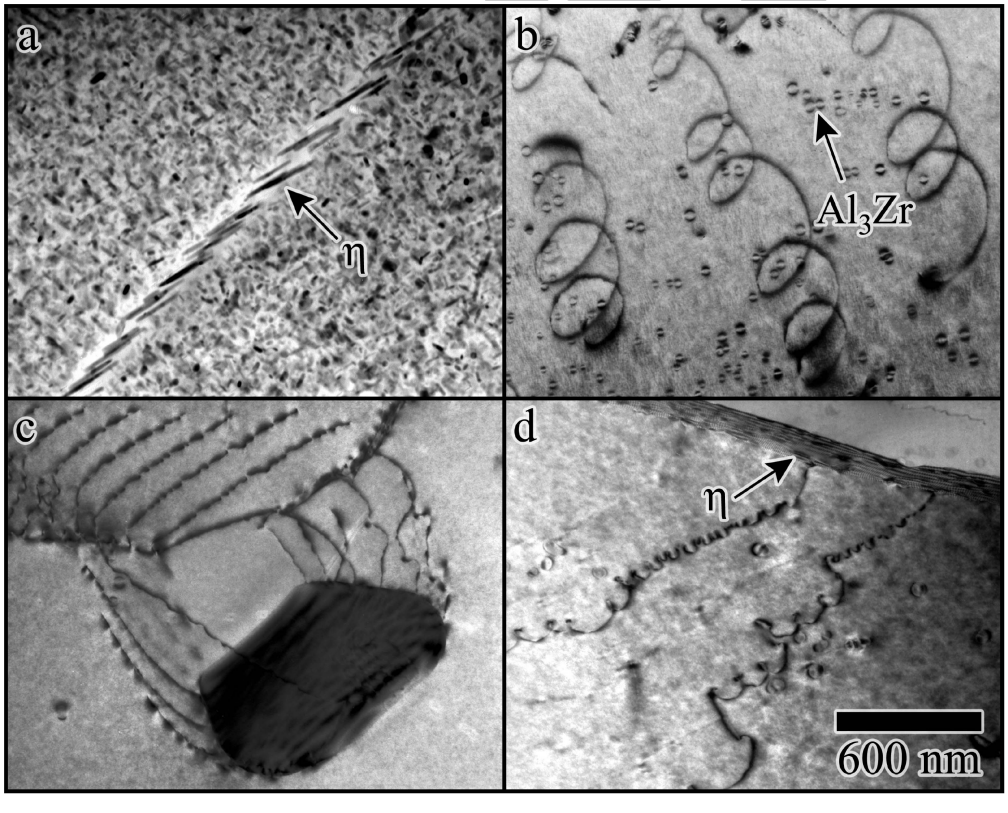

Fig. 1—Microstructures of AA7055: (*a*) in the as-received T79 condition; and after homogenizing at 480 °C for 1 h, then holding for 3 min at (*b*) 500 °C, (*c*) 460 °C, and (*d*) 420 °C, and then quenching in water. Dislocations evident in the micrographs are due to residual strain fields in the samples.

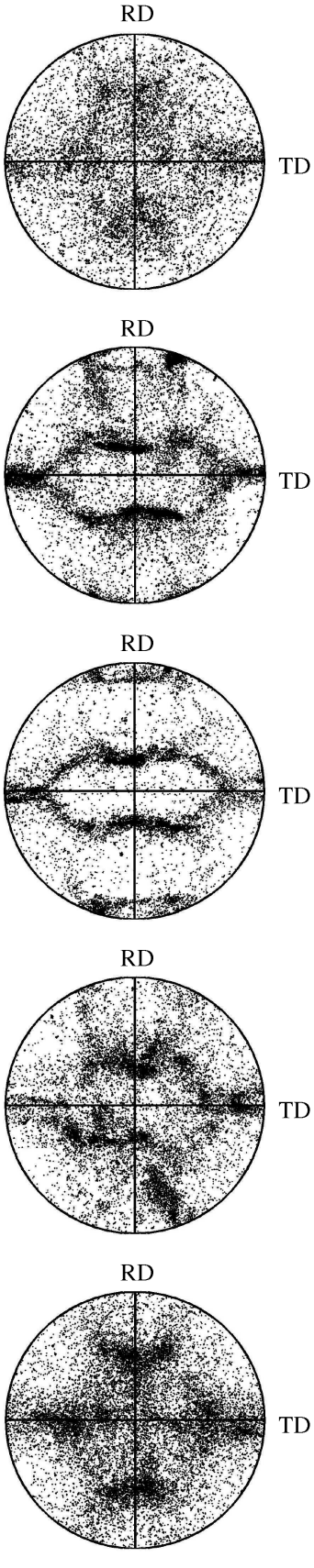

Fig. 2—⟨111⟩ pole figures for as-received AA7055 plate. Starting from the top, the measurements were made on the top surface, *t*/4, *t*/2, 3*t*/4, and bottom surfaces.

nitric acid in methanol at a temperature of −25 °C and a voltage of 10 V. Texture was measured through electron backscattered pattern analysis, which was performed using Oxford Instruments software on a Zeiss DSM-960 scanning electron microscopy. ⟨111⟩ pole figures calculated from these experiments are shown as stereographic projections in Figure 2.

Of particular note is the asymmetry in the texture of the top and bottom surfaces. The bottom surface shows a much stronger ND rotated cube shear texture compared to the top surface. The asymmetry is also evident in the texture at the quarter planes. The midplane, as expected, is representative of plane-strain compression deformation. The asymmetry in the experimental texture suggests a corresponding asymmetry in the rolling process. This has important implications for the development of our numerical model of the rolling process, which must be able to capture this asymmetry.

Given our focus on hot rolling, comment on the relevance of texture for as-received plate to that developed relatively early in thermomechanical history for the product is warranted. In a detailed study of 7010 plate, Engler *et al*.[8] provide evidence that the recrystallized texture contains a random component associated with particle-stimulated nucleation (PSN), while recovery of subgrain structure tends to sharpen the original deformation texture. As indicated previously, Zr addition to the alloy suppresses development of recrystallization components. The net effect is that for our material, the bulk texture developed in hot rolling and final texture following solution heat treatment are quite similar. The occurrence of PSN is also indicated in 7050 plate.[2] From the standpoint of the current effort, this is a fortuitous circumstance: comparison of measured crystallographic texture from the final product with simulated texture is possible by virtue of this mechanism of texture preservation. We return to this point in the section on the hot rolling model, after first describing the development of a constitutive model for hot deformation.

III. MECHANICAL TESTING

A mechanical testing program was undertaken to develop constitutive relations suitable for modeling hot rolling. We performed uniaxial compression tests on samples following a thermomechanical protocol similar to the industrial process. The testing apparatus and specimen geometry are shown schematically in Figure 3. The tests were performed in

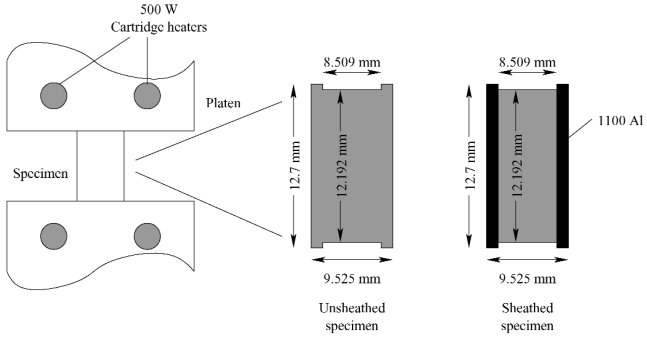

Fig. 3—Schematic of test rig and specimen.

a hydraulic load frame with Instron 8500 controls. Temperature control was effected using INCONEL† platens fitted with 500-W cartridge heaters, water-cooled jackets, and type-K thermocouples, controlled by Omega CN2011 controllers.

†INCONEL is a trademark of INCO Alloys International, Huntington Woods, WV.

The samples were upright cylinders, machined from the as-received hot-rolled plates with the compression axis aligned with the rolling direction. The cylinders had a recess machined in each end (Figure 3), which was filled with a 2:1 mixture of vacuum grease and colloidal graphite prior to testing.[9] Compression tests were run on these samples at two different constant crosshead velocities, corresponding to an approximate strain rate of 10^{-3} s^{-1} or 1 s^{-1}.

A second purpose for carrying out these high-temperature deformation studies was to assess the evolution of damage, manifested as porosity beginning in grain boundaries, observable by metallographic examination of the deformed specimens. This porosity is thought to be associated with melting of some of the residual secondary phases and extended by deformation. During very high-temperature deformation, the material tended to come apart during compression along grain boundaries by coalescence of pores, as shown in Figure 4(a). To preserve specimen integrity under such conditions, a modification of the specimen design was made, whereby the test material was press fit into a thin-walled sheath of 1100 aluminum. The sheath, due to its thin wall, provides minimal containment on the core specimen, as seen in Figure 4(b). The axial stress in the sheath can be subtracted from the measured total stress to reveal the response of the core.

Following industrial practice, and consistent with our differential scanning calorimetry (DSC) measurements of the dissolution of ? phases, specimens were homogenized at 480 °C for 1 hour. After this treatment, the platen and specimen were brought to the desired test temperature in the range from 380 °C to 500 °C over a time of 3 to 5 minutes, and then held at that temperature for 3 minutes prior to compression. The total time near the test temperature (equilibration + hold time) was from 5 to 8 minutes. Immediately following compression, samples were removed from the platens and quenched in cold tap water.

Measured true stress–true strain curves from these tests are shown in Figure 5. The strain shown has had the elastic response of the material and the load frame subtracted. No hardening is observed, and after about 2.5 pct strain, the material flows at constant saturation stress, which depends on temperature and strain rate. Cerri *et al.*[10] reported similar behavior in hot torsion testing up to 400 °C of 7012 and 7075 alloys, as did Sheppard and Wright[11] for dilute aluminum alloys at temperatures up to 500 °C.

Our compression data can be correlated by fitting the data to a power-law steady-state creep model:[12]

$$\frac{S_{sat}}{\mu(T)} = A_0^{1/n}\left[\dot{\varepsilon}\exp\left(\frac{Q_D}{RT}\right)\right]^{1/n} \qquad [1]$$

where $\mu(T)$ is the shear modulus as a function of temperature T;[13] $\dot{\varepsilon}$ is the strain rate; Q_D is the activation energy for diffusion, taken to be 120 kJ/mol corresponding to the diffu-

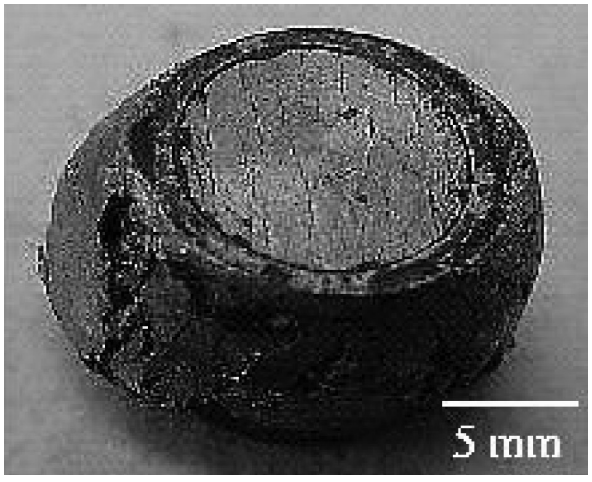

(*a*)

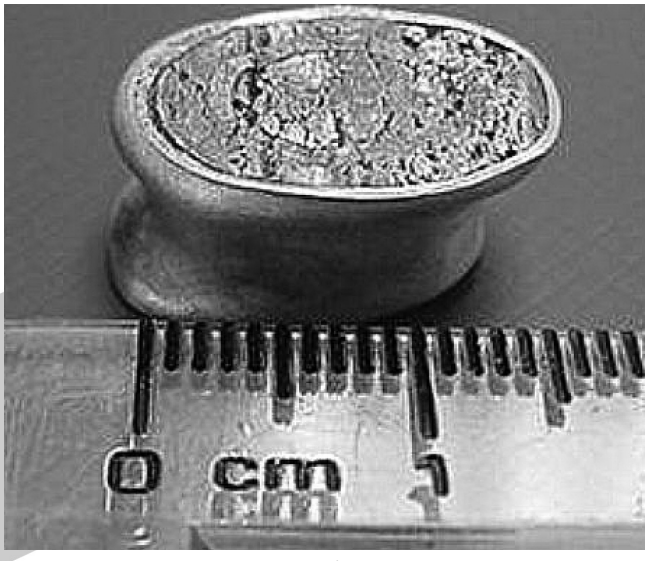

(*b*)

Fig. 4—Compression sample design evolution—addition of 1100 aluminum sheath provides containment at higher temperatures: (*a*) original specimen design and (*b*) sheathed specimen design.

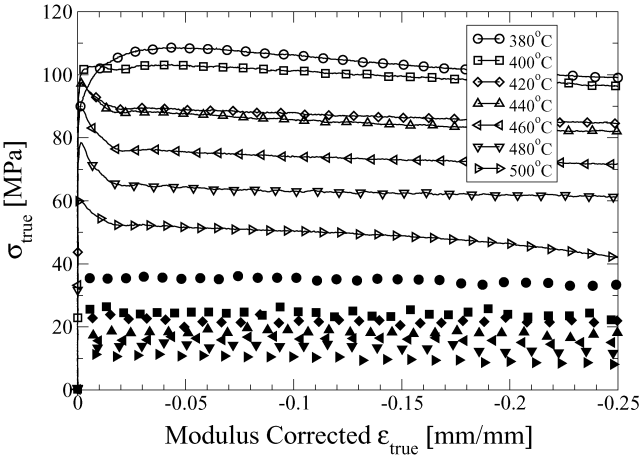

Fig. 5—Mechanical behavior of homogenized AA7055. Filled symbols are for tests with $\dot{\varepsilon} = 10^{-3}$ s^{-1}, and open symbols are for tests with $\dot{\varepsilon} = 1$ s^{-1}. The symbol shape indicates the testing temperature.

sion of Zn in Al;[14] and R is the ideal gas constant. We refer to the quantity in square brackets in Eq. [1] as ζ, the temperature-compensated strain rate. The terms A_0 and n are model constants, which can be extracted by plotting the experimentally measured σ_{sat}/μ *vs* ζ on logarithmic scales, as shown in Figure 6. Also included in this figure are tensile data for 7050 reported by Ghosh,[15] previously unpublished results from hot torsion tests on 7050 from Giardina,[16] and data from Sheppard *et al*. on 7075.[17] It can be readily seen that the response of all three alloys is quite similar.

The data fall into three regimes. For $\zeta < 5$, we find $n = 1.2$, and for $5 < \zeta < 9$, $n = 4.47$. The latter region is commonly referred to as "five-power-law" creep.[12,18,19] When $\zeta > 9$, we find $n = 10.2$. We will see later that during hot rolling, nearly all of the deformation takes place in this latter regime. One would expect a progression into a "power-law breakdown" regime for the homogenized material as stress is increased through higher strain rate. However, for consistency with crystal plasticity simulations to be described, we will adopt the phenomenological characterization through a power law. Specifically, both simulation of viscoplastic flow in rolling and evolution of texture (as a postprocessing operation) will be conducted using a power-law form with identical stress exponent. We also tested a few samples with the compression axis oriented along the normal to the rolling direction. The results from these tests, indicated as "ND" in Figure 6, are indistinguishable from the tests conducted with the specimen axis parallel to the rolling direction. This indicates that although the rolling process itself is constrained by kinematics, the material response is isotropic.

Samples from the tests performed with $\dot{\varepsilon} = 1\ s^{-1}$ at 420 °C, 450 °C, 455 °C, 460 °C, 480 °C, and 500 °C were prepared *via* scanning electron microscopy (SEM) in order to examine the evolution of internal damage. Three orthogonal cuts were made with a diamond saw to expose surfaces whose normal was in the rolling direction (RD), perpendicular to the rolling plane (ND), and in the transverse plane (TD). The surfaces were polished, etched, and imaged using a procedure similar to that described for the specimens used in texture measurements.

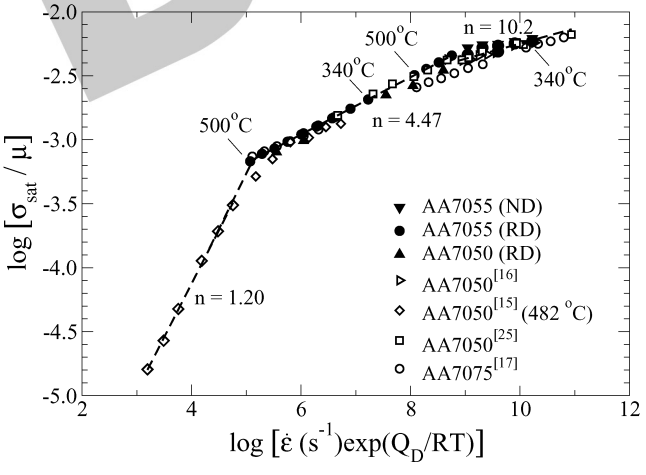

Fig. 6—Saturation stress, normalized by shear modulus, *vs* temperature-compensated strain rate for compression tests in this work (solid symbols), torsion tests by Giardina,[16] tension tests by Ghosh,[15] compression tests by Hander,[28] and results for 7075 from a correlation by Sheppard *et al*.[17]

The SEM images from deformed specimens, shown in Figure 7, indicate that localized damage begins to appear in specimens deformed at 455 °C and above, as dark spots at grain boundaries. At 480 °C, in Figure 7(e), similar dark spots show distinct linear arrangements. In Figure 7(f), from compression at 500 °C, there is a rippled edge to each microcrack, as if multiple voids had coalesced to form the elongated crack. The voids appear aligned in distinct patterns and show both increased frequency and severity with increasing temperature of deformation. Note also that the micrographs from all of these samples clearly show that the original elongated grains remain, and that there has been no recrystallization during heat treatment or deformation.

In Section IV, the measured constitutive relation is implemented in a numerical model for hot rolling. The fact that the material can be characterized by the saturation stress at any particular temperature and strain rate permits modeling the material as a non-Newtonian fluid. The tests presented in this section also clearly show that damage begins to occur in the material when it is deformed at temperatures above about 455 °C. We will therefore look for rolling conditions that lead to this undesirable state.

IV. ROLLING MODEL

To model the hot rolling process, we follow a two-step procedure. We first compute the velocity, temperature, and pressure fields using a material model, which is derived from the mechanical property measurements. A subsequent post-processing step is executed to derive through-thickness texture evolution from the computed velocity field. We emphasize that the kinematic constraints imposed by the boundary value problem for rolling and the relatively rate-sensitive, nonhardening material response allow for this sequential treatment of the thermomechanical problem and texture evolution. This is a relaxation of the more rigorous, fully coupled approach advanced by Mathur and Dawson[20] for analysis of cold rolling a rate-insensitive workhardening material. As a practical consequence, the (much) reduced computational overhead in the decoupled approach allows for timely study of multipass rolling, as well as parametric studies of friction and heat transfer, to be detailed subsequently.

The compression tests show that, in the temperature range of interest for hot rolling, the material flows at constant stress σ_{sat} once the strain exceeds 2.5 pct. Because the strains experienced in hot rolling are considerably higher than this value, the material can be modeled as an incompressible viscous fluid, with viscosity a function of strain rate and temperature derived from the constitutive relation in Eq. [1]. Considering the material to be a non-Newtonian fluid permits the use of a commercial computational fluid dynamics package FIDAP‡ to model the hot rolling process.

‡FIDAP is a trademark of . . .

The material is modeled as an incompressible, purely viscous, non-Newtonian fluid obeying the constitutive relation:

$$\tau = 2\Lambda(\dot{\varepsilon}, T)\, D \qquad [2]$$

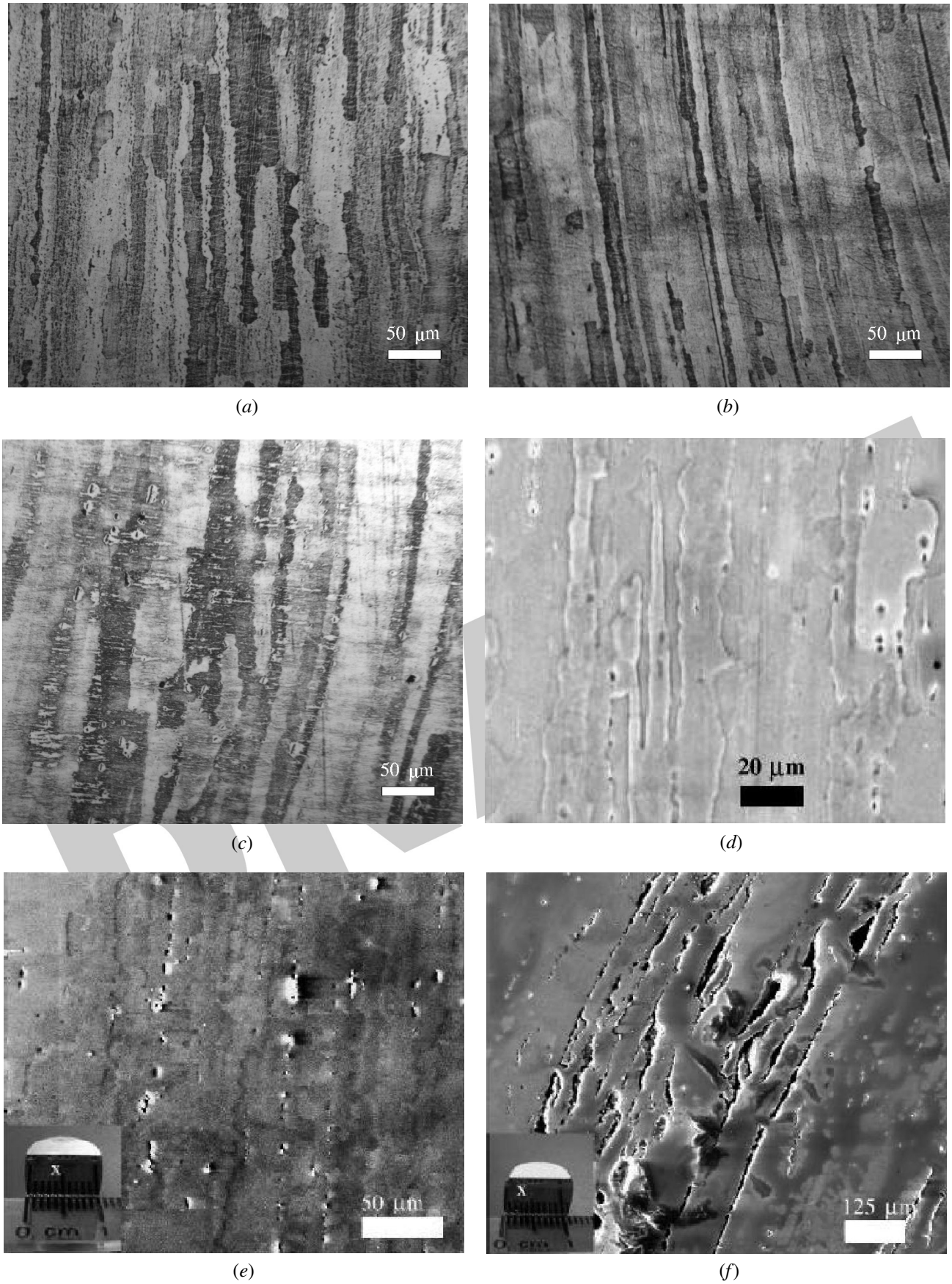

Fig. 7—Microstructures from homogenized 705 times compressed at various temperatures at a strain rate of 1 s^{-1}: (*a*) 420 °C, (*b*) 450 °C, (*c*) 455 °C, (*d*) 460 °C, (*e*) 480 °C, and (*f*) 500 °C.

Here, Λ is the non-Newtonian viscosity; τ and D are the deviatoric stress and rate of defor-mation tensors, respectively; and the effective strain rate $\dot{\varepsilon}$ is defined as

$$\dot{\varepsilon} = \sqrt{(2/3)D:D} \quad [3]$$

By contracting τ with itself, a scalar form for Eq. [2] can be found

$$\tau = 3\Lambda(\dot{\varepsilon}, T)\,\dot{\varepsilon} \quad [4]$$

where $\tau = \sqrt{(3/2)\tau:\tau}$ is the scalar magnitude of τ. This form permits the behavior of the material in a three-dimensional stress state to be determined form the uniaxial compression response, with the non-Newtonian viscosity Λ given by

$$\Lambda = \frac{S_{\text{sat}(\dot{\varepsilon},T)}}{3\dot{\varepsilon}} \quad [5]$$

where $S_{\text{sat}(\dot{\varepsilon},T)}$ may be computed from the constitutive relation in Eq. [1].

The viscosity model is implemented as a user subroutine in FIDAP. Within each element, D is computed at each integration point using the putative velocity solution, from which $\dot{\varepsilon}$ is computed using Eq. [3]. The combination of $\dot{\varepsilon}$ and T yields the local saturation stress from Eq. [1], and substitution of this value of σ_{sat} into Eq. [5] gives the local viscosity. Note that as the strain rate approaches zero, the viscosity computed from Eq. [5] is unbounded. Using a maximum cutoff viscosity of 100 MPa·s gave good numerical stability, and the simulation results were unaffected by small changes in this limiting value. The velocity solution is then found using these viscosity values, and the procedure is iterated to convergence.

The final four reversing passes were simulated, assuming two-dimensional, steady-state conditions. In these four passes, plate thickness is reduced from 127 to 25.4 mm with a constant 25.4-mm draft in each pass. A representative finite-element mesh, corresponding to the second pass, is shown in Figure 8. Geometrically, similar meshes were used in the deformation zone for each pass, with dimensions reduced accordingly. Sufficient entry and exit lengths were included such that the computed results were independent of the cutoff points. The rolls are not included in the simulations, but are represented by their respective tangential velocities in the roll bite. Additional boundary conditions are also indicated in Figure 8. Note that symmetry is not imposed at the midplane, and that, based on experimental observations, the

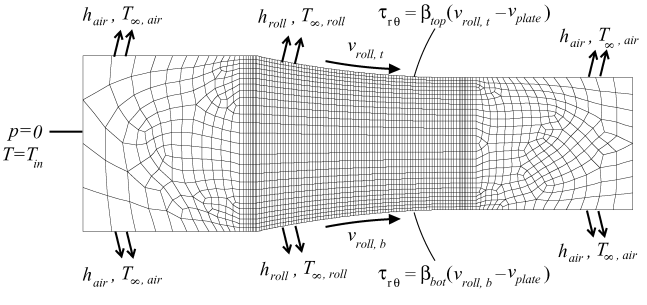

Fig. 8—Finite-element mesh for pass 2, in which thickness is reduced from 101.6 to 76.2 mm. General boundary conditions are shown specified independently on the top and bottom surfaces.

various coefficients are specified independently on the top and bottom surfaces.

Following Mathur and Dawson,[21] friction at the roll/plate interface is modeled using a slip model, where the shear stress is assumed to be proportional to the difference between the roll surface speed v_{roll} and the local tangential surface speed of the plate $v_{\text{plate},viz}$.

$$\tau_{r\theta} = \beta(v_{\text{roll}} - v_{\text{plate}}) \quad [6]$$

The slip coefficient β is a simulation parameter, representing lubrication conditions, that controls the relative slip between the roll and plate. Higher values of β correspond to less slip, and higher shear stresses along the arc of contact. The model accommodates different values for β on the top and bottom surfaces.

Heat transfer on the external surfaces is modeled by means of a convection boundary condition. Industrial plant measurements suggest a heat-transfer coefficient, h_{air}, of 0.85 kW/m^2 K for coolant-covered surfaces of the plate exposed to air, corresponding to the region outside the roll bite.[22] Heat-transfer coefficients between the plate and roll, h_{roll}, have been reported to range from as low as 9.3 kW/m^2 K for cold rolling of commercially pure aluminum[23] to as high as 450 kW/m^2 K for hot rolling of AA5000 series alloys.[24] The computed texture was relatively insensitive to the value of h_{roll} when it was in the range 10 to 60 kW/m^2 K. For the simulations described in detail below, we used $h_{\text{roll}} = 21$ kW/m^2 K, a figure suggested by plant measurements.[22]

For each pass, the inlet temperature was set to the lay-on temperature of 427 °C. Setting the inlet temperature to be the same for each pass assumes that convective heat losses balance viscous dissipation in each pass, a common industrial practice. This condition was verified postsimulation by computing the average exit temperature of the plate cross section, which was found to deviate by at most + 10 °C (+1.5 pct) from the lay-on temperature in the simulations.

Grid converged solutions were found using a relatively fine mesh in the deformation zone, containing 1950 elements graded toward the roll boundaries. The fine mesh also extends eight elements outside the roll bite in each direction. The remaining mesh outside the roll bite is coarser, containing a total ranging from 916 to 1047 elements for the four passes depending on inlet and outlet thickness. Interior elements are nine-noded isoparametric quadrilaterals with quadratic velocity and continuous linear pressure interpolation. The boundaries consist of three-noded quadratically interpolated isoparametric elements. Pressure is set to zero at the inlet. On average, 23 iterations were required to achieve convergence of the solution, using successive substitution to resolve the nonlinearities. Convergence was declared when the root-mean-square value of the residual and the relative change in solution vectors normalized by their respective initial values were each less than 10^{-4}.

An extensive set of simulations was performed to explore the role of the various process parameters. Detailed results are presented for one parameter set, given in Table I, which produced simulated textures most closely matching those measured experimentally, shown in Figure 2. The sensitivity of the results to the input parameters is discussed as variations from this case. Of particular note, the slip coefficients on the top and bottom are 250 and 350 MPa/m/s, respectively,

corresponding to larger shear forces at the bottom, as suggested by experimental textures. All other parameters are the same at the upper and lower surfaces of the plate.

Figure 9 depicts the computed shear rates for all four passes modeled. The effect of the differential slip coefficients is manifested as an asymmetry in the shear rate distribution, with more shear along the bottom of the plate, where β is larger. The deformation is also shown to be nonhomogeneous, localizing along lines of maximum shear at about 45 deg to the RD. This localization is to be expected, because our constitutive relation (Eq. [1]) resembles a shear-thinning power-law fluid with power-law exponent $1/n < 1$. As the aspect ratio of the deformation zone increases, the number of localized lines increases along with the average strain rate.

Figure 10 shows the shear stress in the plate at the roll/plate interface. Note that the slip model we have chosen ensures that the effective stress in the material does not exceed the saturation stress, without the need for capping. The neutral point is indicated in the figure for reference.

Computed pressure contours are shown in Figure 11. The majority of the material is under hydrostatic compression ($p > 0$). However, negative pressures, or regions of hydrostatic tension, are found at the entrance and exit of the roll bite. Note that these negative pressures are due to local accelerations, and do not derive from elastic unloading, as the material model is purely viscoplastic. Regions of hydrostatic tension are of particular interest because any defects present in the material tend to grow under such conditions. At least some of the negative pressure is an artifact of the slip model inaccurately representing the deformation at these locations.

Table I. Process Parameters for Simulation Results Presented

Parameter	Symbol	Value
Bottom slip coefficient	β_{bot}	350 MPa/m/s
Top slip coefficient	β_{top}	250 MPa/m/s
Tangential roll velocity	v_{roll}	1.17 m/s
Heat-transfer coefficient between roll and plate	h_{roll}	21 kW/m^2 K
Reference temperature for roll	$T_{\infty,roll}$	94 °C
Heat-transfer coefficient between air and plate	h_{air}	0.85 kW/m^2 K
Reference temperature for air	$T_{\infty,air}$	25 °C
Lay-on temperature	t_{in}	427 °C

The temperatures in each pass show similar characteristics. However, the maximum temperature increases with increasing reduction ratio due to greater viscous work. The computed temperature field for pass 4 (the final pass) is shown in Figure 12. The majority of the material at any given vertical cross section is nearly isothermal. A thin, cooler layer exists near the surface in the roll bite, where the gradient is high due to the large heat-transfer coefficient. The maximum temperature is about 462 °C, which corresponds to the temperature at which damage began to appear in the compression samples. The average temperature at the roll exit for passes 1 through 4 was 434 °C, 435 °C, 439 °C, and 450 °C, respectively. These results indicate that using the same lay-on temperature for each pass is reasonable. The temperature distribution within the plate is discussed further subsequently, when the sensitivity of the model results to the value of heat-transfer coefficient is examined.

With the velocity field in hand, texture evolution through the rolling process can be computed using a viscoplastic self-consistent (VPSC) polycrystal plasticity code.[21,25] Within VPSC, each grain in the polycrystal is treated as an inclusion in a homogeneous effective medium whose properties are determined from the bulk average. The response of each grain obeys a power-law constitutive form, where the rate sensitivity is specified as 10.2, consistent with our experimental measurements. At each time-step, texture is updated based on the imposed deformation, slip system shear strengths, and current texture. To determine the imposed deformation, a set of 500 randomly oriented massless particles is introduced at the inlet, and their motion is integrated through time using the computed velocity field. These data provide the velocity gradients necessary to evolve the texture along streamlines. Texture is evolved continuously through the final four passes, *i.e.*, the texture computed after pass 1 is used as the initial texture for pass 2 and so on. While simulations of rolling passes were performed with the "left-to-right" flow of material, as indicated in Figures 9 through 11,

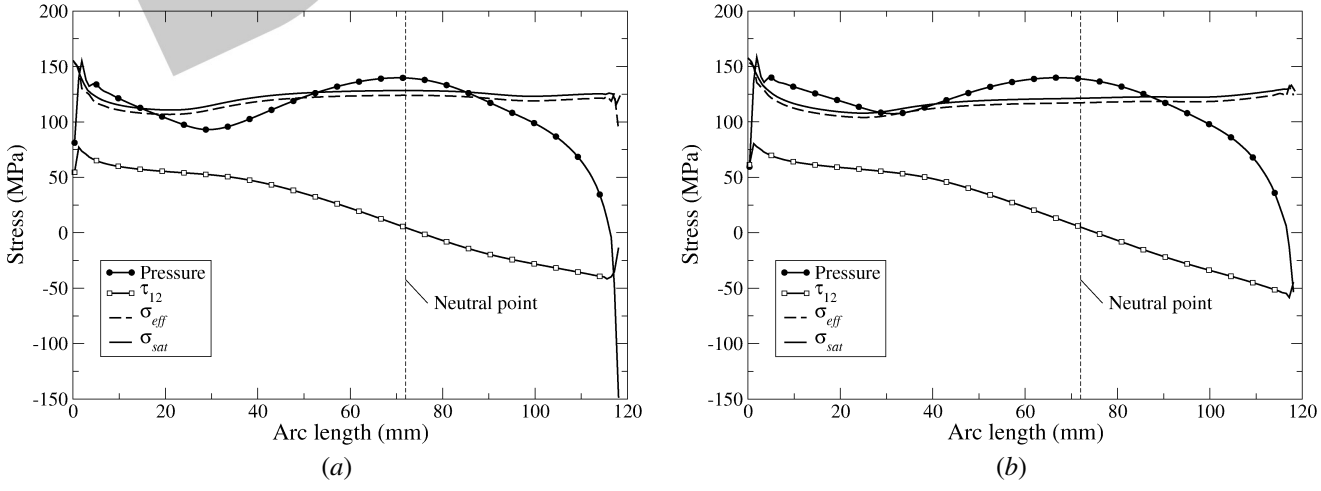

Fig. 10—Computed shear stress, saturation stress, and pressure along the arc of contact for the upper and lower rolls in pass 4: (*a*) top roll surface and (*b*) bottom roll surface. The total normal stress is also shown.

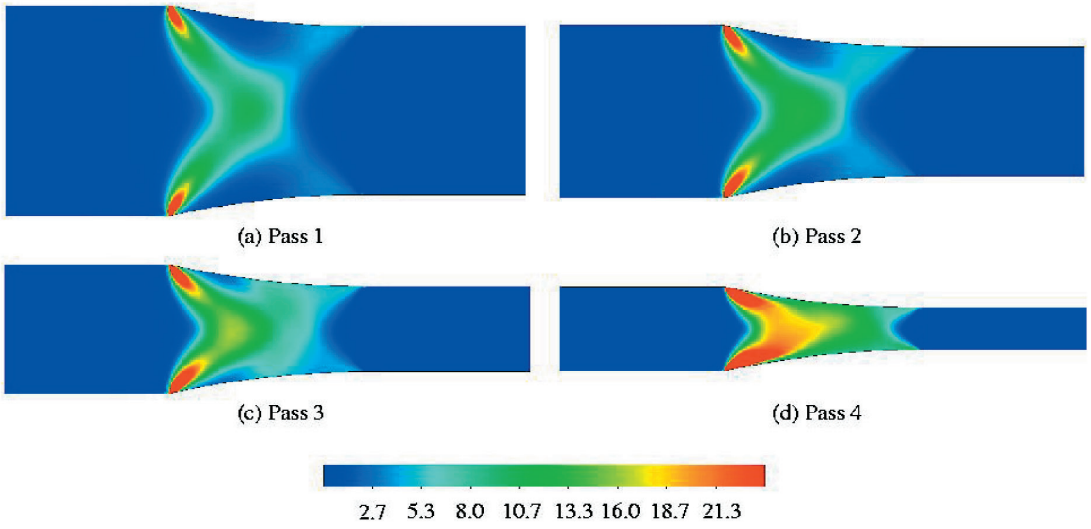

Fig. 9—Computed shear rate (s^{-1}) computed for each pass. Note the top-to-bottom asymmetry, especially in pass 4: (*a*) pass 1, (*b*) pass 2, (*c*) pass 3, and (*d*) pass 4.

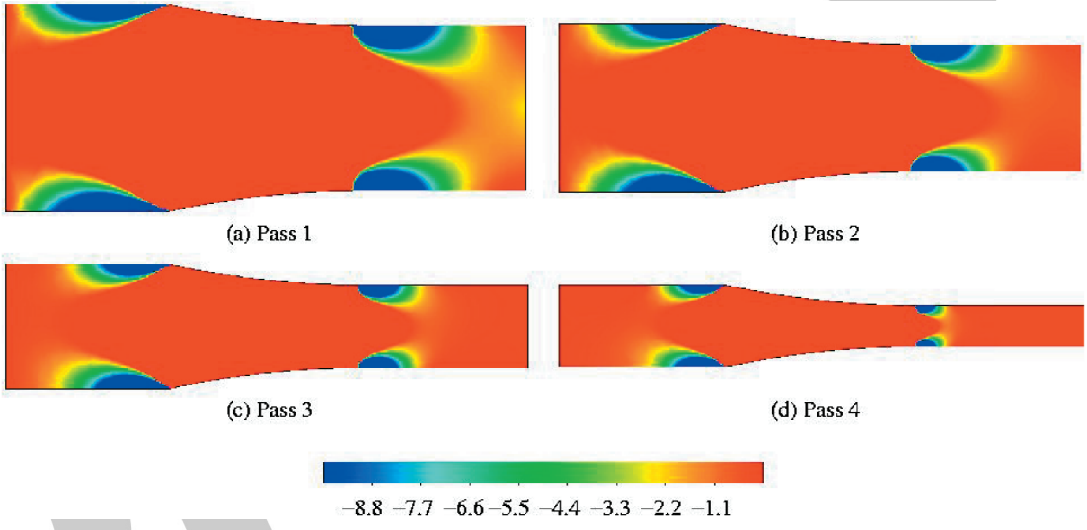

Fig. 11—Computed pressure distribution (MPa) for each pass: (*a*) pass 1, (*b*) pass 2, (*c*) pass 3, and (*d*) pass 4.

the resulting velocity gradients were modified (through sign change of off-diagonal components) to simulate texture evolution in reversing passes.

Figure 13(b) shows simulated ⟨111⟩ pole figures after pass 4 for the process parameters outlined in Table I. Simulated textures match quite well to experimental measurements, reproduced from Figure 2 in Figure 13(a) for comparison. At the bottom surface, a strong shear texture is predicted. The simulated top surface texture matches closely to experimental measurements, with a slightly greater rotation about the TD in the simulations. Simulated textures at the quarter and half planes also very closely resemble experimental measurements. At the midplane, a plane strain compression texture is observed, as expected for rolling processes. Note that whereas in cold rolling friction between the plate and rolls can be measured indirectly through roll torque, this does not work well in hot rolling, where the frictional forces represent a much smaller fraction of the total torque in the mill. Thus, it is essential to use indirect means, such as the texture, as an indication of the thermomechanical history of the plate. Some of the model parameters such as roll diameter, roll speed, and lay-on temperature were chosen to model a desired pass schedule. In contrast, the slip coefficients and heat-transfer coefficients are very difficult to measure experimentally; a parametric study was performed to determine the sensitivity of the computed results to variations in these parameters.

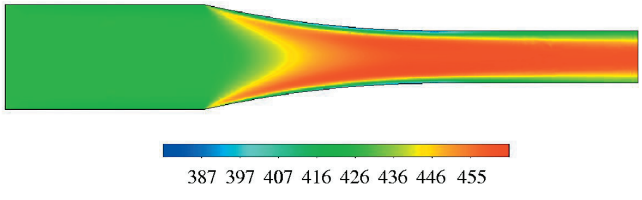

Fig. 12—Computed pass 4 temperature distribution (°C) with a lay-on temperature of 427 °C.

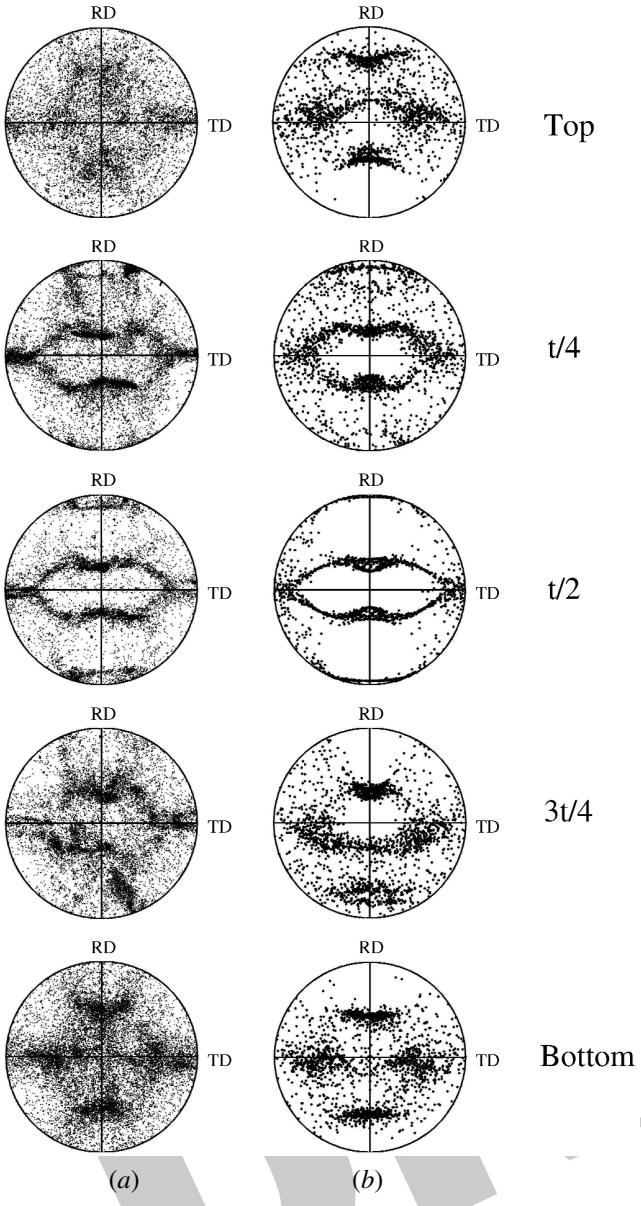

Fig. 13—⟨111⟩ pole figures: (*a*) experimental and (*b*) simulated texture for model parameters listed in Table I.

The simulated texture is very sensitive to the values of the slip coefficients. To illustrate this point, the results of simulations using symmetric values for β of 150 and 300 MPa/m/s, respectively, are shown in Figures 14(a) and (b). For these two cases, the heat-transfer coefficients were the same as in the simulations reported previously, where $h_{roll} = 21$ kW/m^2 K. When the smaller value of β is used, a plane-strain compression texture extends through the majority of the plate. Additionally, the 45-deg ND rotated cube shear texture is absent at the surface, which is inconsistent with the experimental measurements reported earlier. Using a higher value of β produces the 45-deg ND rotated cube shear texture at the surface.

Note that the adjustment of the frictional conditions through assessment of texture offers a useful alternative to tuning them through comparison to roll force or torque. In hot rolling of aluminum, roll force and torque are dominated by reduction, whereas the contribution due to lubrication conditions is difficult to assess—with a complex (and offsetting) interplay between heat transfer, viscous heating, and lubrication.[26] From the practical standpoint, friction and heat-transfer coefficients are difficult to measure in the production environment. Validating a model through comparison to a roll torque integrates model details into a single parameter the relative contribution of underlying factors, such as changes in lubricant behavior, metal constitutive response, and heat transfer with speed for example, is obfuscated. In contrast, comparison of predicted and measured texture reveals the degree to which one captures gradients in the boundary value problem that serves as an idealization of the rolling operation. Faithful reproduction of such gradients supports the notion that boundary conditions and nonlinear material response are well represented in the model.

Forward slip also provides a secondary check as to whether the model results are reasonable. We find that in the four passes model, corresponding to reductions of 20, 25, 33.3, and 50 pct, the computed forward slip values for the base case are 3.4, 5.1, 7.7, and 14.5 pct, respectively. These predictions are consistent with the experimental measurement of forward slip reported in the literature for the hot rolling of pure aluminum strip.[26,27]

Simulated textures proved to be relatively insensitive to variations in the h_{roll} in the range of 10 to 60 kW/m^2 K. This is illustrated in Figure 14(c), which shows almost no change in simulated texture for the case $h_{roll} = 60$ kW/m^2 K and $\beta = 300$ MPa/m/s. Figure 15 shows the plate exit temperature across the thickness after pass 4 for different values of h_{roll}. Although the maximum temperature is essentially unaffected by h_{roll}, the location of the maximum temperature shifts toward the midplane with increasing h_{roll}. Also note that asymmetric specification of β results in a slightly higher maximum temperature in the bottom half of the plate. The effects of viscous heating are evident as the maximum temperature exceeds 460 °C, at which the onset of damage is suggested in our compression tests. Note also that the position of the maximum temperature point moves toward the center of the plate as h increases. This may afford the material further protection from failure.

Examination of simulation results provides an *a posteriori* consistency check of the model. The accumulated strain exceeds 2.5 pct everywhere in the plate almost immediately upon entering the deformation zone. This makes it reasonable to model the material using the purely viscoplastic model derived from experimental saturation stress data. The temperature-compensated strain rate ζ can be computed from the final solution. These data show that virtually the entire deformation zone falls within the range where $1/n = 10.2$, consistent with the value used in VPSC to compute the texture evolution. A small portion of the material, near the entrance to the roll bite, has values of the temperature-compensated strain rate outside the range of our experimental measurements. The constitutive model was extrapolated for these locations.

V. DAMAGE MODELING

Our ultimate goal in this work is to quantitatively define the thermomechanical processing window. We propose a damage parameter that incorporates our experimental observation that damage first appears when deformation is carried

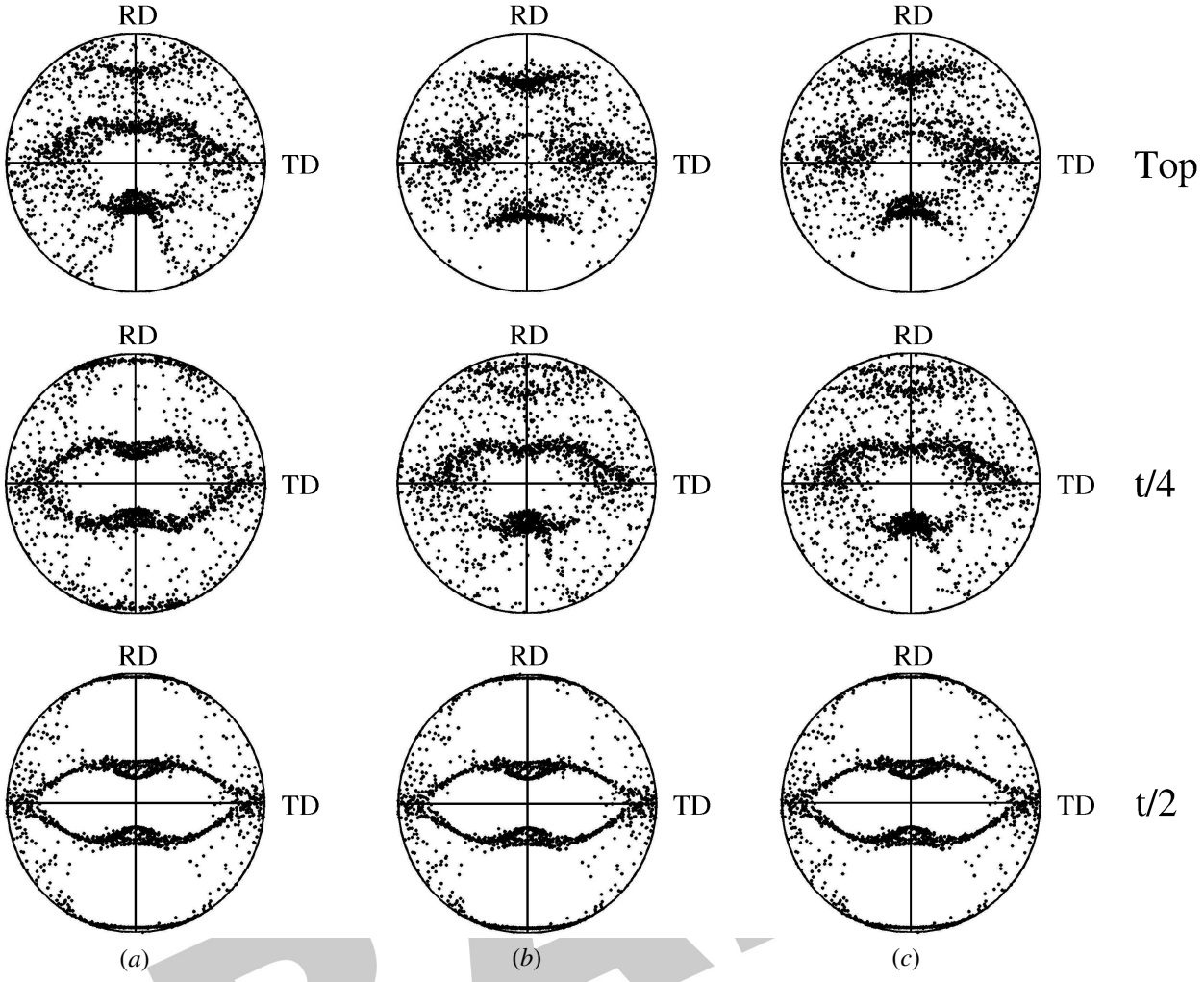

Fig. 14—Simulated ⟨111⟩ pole figures for (*a*) β = 150 MPa/m/s, h_{roll} = 21 kW/m^2 K; (*b*) β = 300 MPa/m/s, h_{roll} = 21 kW/m^2 K; and (*c*) β = 300 MPa/m/s, h_{roll} = 60 kW/m^2 K.

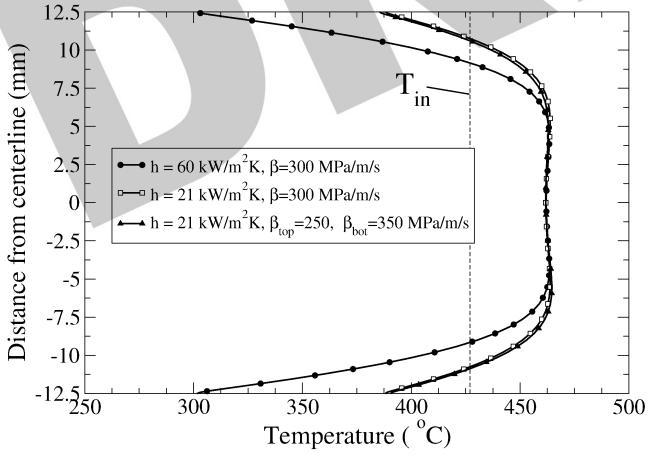

Fig. 15—Pass 4 exit temperature profile.

out above 455 °C, and increases with increasing temperature; and that the probable deformation mechanism is shearing along grain boundaries. To that end, we define

$$? = \oint_s t_{max}\, A(T) ds \qquad [7]$$

where S is a streamline, τ_{max} is the magnitude of the maximum shear stress at any point along the streamline, and $A(T)$ is given by

$$A(T) = \begin{cases} 0 & T \le 455 \\ T - 455 & T > 455 \end{cases} \qquad [8]$$

This parameter is readily computed from the data already extracted to compute the texture. Figure 16 shows the computed damage field for the final pass with ν_{roll} = 1.17 m/s. Note that for this roll speed, the final pass was the only pass in which the temperature exceeded 455 °C anywhere in the plate. Figure 17 shows the accumulated damage at the exit of the deformation zone for various roll speeds. Note that damage, as measured by this criterion, is found even at relatively low roll speeds. The maximum value of χ increases with roll speed, and its location shifts from $t/4$ for ν_{roll} = 0.94 m/s to nearly $t/10$ for ν_{roll} = 1.5 m/s. In order to eliminate the possibility of damage during hot rolling, process parameters must be chosen such that temperatures do not reach 455 °C. For the case studied here, that corresponds to running at $\nu_{roll} < 0.4$ m/s. Alternatively, smaller reductions may be taken in final passes. Further experimental work is required to determine a threshold value of χ, in order to make full use of the model in defining the TPW and optimizing the hot rolling process.

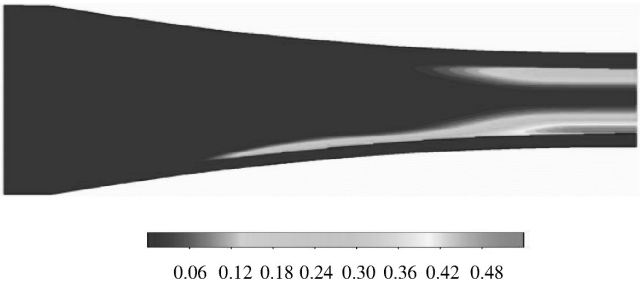

Fig. 16—χ damage field for pass 4 with $?_{roll}$ = 1.17 m/s.

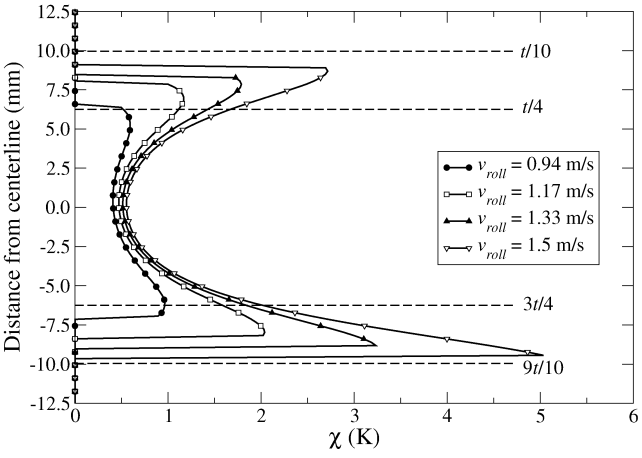

Fig. 17—χ damage parameter at roll exit for various roll speeds.

VI. DISCUSSION AND CONCLUSIONS

Microscopy and DSC results indicate a significant presence of strengthening precipitates in the as-received material. Industrial processing includes a homogenization at 480 °C prior to hot rolling, which dissolves all but Al_3Zr secondary phases. The Al_3Zr particles act as inhibitors to recrystallization during hot deformation.

Isothermal compression tests were performed on AA705X specimens first homogenized at 480 °C, then cooled/heated to various temperatures ranging from 380 °C to 500 °C, at nominal strain rates of 10^{-3} s^{-1} and 1 s^{-1}. The material saturates at strains of approximately 2.5 pct, so we may use the saturation stress to describe the material response under hot rolling conditions. The correlation of saturation stress with temperature-compensated strain rate yields three distinct regions corresponding to Harper–Dorn creep (n = 1.2), five power-law creep (n = 4.6), and a high stress region (n = 10.2). Microscopy on postcompression specimens illustrates the possible onset of damage at 460 °C and the progression to significant microdamage at 500 °C, thus fixing an upper limit to the TPW.

The derived mechanical constitutive relation has been implemented into a numerical rolling model as a non-Newtonian viscosity. Model parameters, such as roll slip coefficients and heat-transfer coefficients, were tuned through comparison of simulated and experimental textures. Simulated texture was shown to be relatively insensitive to heat-transfer coefficients and very sensitive to friction coefficients. Simulated textures were found to match quite well to experimental textures when asymmetric values of β were used. Shear rate data illustrate the inhomogeneous deformation and asymmetry due to differential friction constants top and bottom.

The asymmetry induced by differential friction leads to localized shearing in the exit region that is greater near the bottom surface than the top for the final pass (Figure 9(d)). Deformational heating during hot rolling was shown to produce maximum temperatures above those at which damage was observed in mechanical testing. This suggests (qualitatively) the potential for subsurface damage near the plate bottom. Looking forward, the collective effort of

1. microscopic and mechanical documentation of homogenized structure,
2. experimental identification of conditions leading to the onset of damage,
3. and exercise of a rolling model with specification of boundary conditions consistent with evolution of material state forms the basis for quantitative study of damage through the introduction of appropriate evolutionary relations.

ACKNOWLEDGMENTS

The microscopy presented in this work was performed in the Center for Microanalysis of Materials, University of Illinois, which is partially supported by the United States Department of Energy under Grant No. DEFG02-91-ER45439. The load frame setup and compression platens were designed and built by Michael Bange. We thank Sally Jankowsky, Alcoa, for her assistance in conducting the DSC analysis. We also appreciate the support of our sponsors, the United States Department of Energy (Grant No. DOE DEFC07–01ID14190) and Alcoa.

REFERENCES

1. S.M. Miyasato, G.H. Bray, J. Liu, and J.T. Staley: "Aluminum Alloy Products Suited for Commercial Jet Aircraft Wing Members," U.S. Patent 5,685,911, Feb. 2, 1999.
2. D. Dumont, A. Deschamps, and Y. Brechet: *Mater. Sci. Eng. A*, 2003, vol. 356, pp. 326-36.
3. D. Godard, P. Archambault, E. Aeby-Gautier, and G. Lapasset: *Acta Mater.*, 2000, vol. 50, pp. 2319-29.
4. L.M. Dougherty: Ph.D. Thesis, University of Illinois at Urbana–Champaign, Urbana, IL, 2001.
5. E. Orowan: *Proc. Inst. Mech. Eng.*, 1943, vol. 150, pp. 140-67.
6. A.I. Fedoseev and G. Gottstein: *Proc. 1st Int. Conf. on Modelling of Metal Rolling Processes*, London, 1993, The Institute of Metals, London, 1993, pp. 296-308.
7. B. Beckers, R. Sebald, G. Pomana, D. Gade, and G. Gottstein: *Proc. 19th Risø Int. Materials Science: Modelling of Structure and Mechanics of Materials from Microscale to Product*, Roskilde, Denmark, 1998, Risø National Laboratory, Roskilde, 1998, pp. 219-27.
8. O. Engler, E. Sachot, J.C. Ehrstrom, A. Reeved, and R. Shahani: *Mater. Sci. Technol.*, 1996, vol. 12, pp. 717-29.
9. M.L. Lovato: Los Alamos National Laboratory, Los Alamos, NM, Materials Science Technician 6, personal communication.
10. E. Cerri, E. Evangelista, A. Forcellese, and H.J. McQueen: *Mater. Sci. Eng.*, 1995, vol. A197, pp. 181-98.
11. T. Sheppard and D.S. Wright: *Met. Technol.*, 1979, June, p. 215.
12. M.E. Kassner and M.-T. Per'ez-Prado: *Progr. Mater. Sci.*, 2000, vol. 45 (1).
13. Y.P. Varshni: *Phys. Rev. B*, 1970, vol. 2, pp. 3952-58.
14. *Smithell's Metals Reference Book*, 7th ed., E. Brandes and G. Brook, eds., Butterworth and Co., Oxford, United Kingdom, 1992, pp. 13-16.

15. A. Ghosh: *Atlas of Stress-Strain Curves*, ASM INTERNATIONAL, Metals Park, OH, 2002, p. 443.
16. F.V. Giardina: "Mechanical Test Report," Reynolds Metals Company, 1992.
17. T. Sheppard, P.J. Tunnicliffe, and S.J. Patterson: *J. Mech. Work Technol*., 1982, vol. 6, pp. 313-31.
18. G.E. Dieter: *Mechanical Metallurgy*, 3rd ed., McGraw-Hill, Inc., New York, NY, 1986.
19. E. Kov'acs-Cset'enyi, N.Q. Chinh, and I. Kov'acs: *Mater. Sci. Forum*, 1996, vols. 217–222, pp. 1175-80.
20. K.K. Mathur and P.R. Dawson: *Int. J. Plasticity*, 1989, vol. 5 (1), pp. 67-94.
21. K.K. Mathur and P.R. Dawson: *Int. J. Plasticity*, 1989, vol. 5 (1), pp. 67-94.
22. L.A. Lalli: Alcoa, Inc., Alcoa Center, PA, personal communication.
23. A.A. Tseng, S.X. Tong, S.H. Maslen, and J.J. Mills: *J. Heat Transfer*, 1990, vol. 112, pp. 301-08.
24. C.O. Hlady, J.K. Brimacombe, I.V. Samarasekera, and E. Hawbolt: *Metall. Mater. Trans. B*, 1995, vol. 26B, pp. 1019-27.
25. O. Engler, M.-Y. Huh, and C.N. Tome: *Metall. Mater. Trans. A*, 2000, vol. 31A, pp. 2299-1315.
26. B. Hum, H. Colquhoun, and J. Lenard: *J. Mater. Proc. Technol*., 1996, vol. 60, pp. 331-38.
27. M. Chun and J.G. Lenard: *J. Mater. Proc. Technol*., 1997, vol. 72, pp. 283-92.
28. W. Hander, G. Sarma, and P. Dawson: "Compression Testing of 7050 Aluminum at Elevated Temperatures," Cornell University, Ithaca, NY, Dec. 1984.

Summary of Comments on E-TP-04-193A-4.qxd

Page: 1

Sequence number: 1
Author: showell
Date: 11/12/2004 9:48:16 AM
Type: Note
Au: Zip code?

Sequence number: 2
Author: showell
Date: 11/12/2004 9:48:38 AM
Type: Note
Au: Titles of positions for all authors (former and current where applicable)?

Page: 3

Sequence number: 1
Author: showell
Date: 11/12/2004 9:49:01 AM
Type: Note
Au: Vendor and location?

Sequence number: 2
Author: showell
Date: 11/12/2004 9:49:21 AM
Type: Note
Au: Which particular section?

Page: 4

Sequence number: 1
Author: showell
Date: 11/12/2004 9:49:49 AM
Type: Note
Au: Vendor and location?

Sequence number: 2
Author: showell
Date: 11/12/2004 9:50:10 AM
Type: Note
Au: Is the trademark information correct?

Sequence number: 3
Author: showell
Date: 11/12/2004 9:50:27 AM
Type: Note
Au: Vendor and location?

Sequence number: 4
Author: showell
Date: 11/12/2004 9:51:01 AM
Type: Note
Au: Is anything missing here?

Page: 5

Sequence number: 1
Author: showell
Date: 11/12/2004 9:51:33 AM
Type: Note
Au: Please provide trademark information.

Page: 12

Sequence number: 1
Author: showell
Date: 11/12/2004 9:53:47 AM
Type: Note
Au: Reference 6: Information correct as set?

Sequence number: 2
Author: showell
Date: 11/12/2004 9:54:01 AM
Type: Note
Au: Reference 7: Information correct as set?

Sequence number: 3
Author: showell
Date: 11/12/2004 9:54:16 AM
Type: Note
Au: Reference 9: Year?

Page: 13

Sequence number: 1
Author: showell
Date: 11/12/2004 9:54:35 AM
Type: Note
Au: Reference 15: Closing page number?

Sequence number: 2
Author: showell
Date: 11/12/2004 9:54:49 AM
Type: Note
Au: Reference16: Location?

Sequence number: 3
Author: showell
Date: 11/12/2004 9:55:09 AM
Type: Note
Au: References 20 and 21 are identical. Is a change needed?

Sequence number: 4
Author: showell
Date: 11/12/2004 9:55:29 AM
Type: Note
Au: Reference 22: Location correct? Year of communication?

Online Proofing Guidance Page

FIRST STEP:

Install Adobe Acrobat Reader if you do not already have this or another Acrobat product installed on your computer. You can do this free of charge by connecting to the Adobe site and following the instructions at:

http://www.adobe.com/products/acrobat/readermain.html

SECOND STEP:

Please download and print your PDF file — we recommend that you save this file to disk, rather than opening it from within your Browser.

From a PC:

1. Right-click on the file/article link.
2. Select ‘‘Save Target as’’
3. Select a desired location on your computer to save the file to, and click on ‘‘Save’’
4. Open your PDf file directly with Acrobat Reader or another Acrobat product.
5. Print this file as you normally would with any typical application. Example: Go up to your toolbar, select ‘‘File’’, select ‘‘Print’’.

From a MAC:

1. Hold the mouse button down over the link.
a. In Internet Explorer, select ‘‘Download Link to Disk’’ from the resulting pop-up menu
b. In Netscape, select ‘‘Save this Link as’’ from the resulting pop-up menu
2. Select a desired location on your computer and click on ‘‘Save’’
3. Open your PDF file directly with Acrobat Reader or another Acrobat product.
4. Print this file as you normally would with any typical application. Example: Go up to your menu bar, select ‘‘File’’, select ‘‘Print’’.

THIRD STEP:

Please go through the file you have just printed and thoroughly and clearly mark any revisions you would like to see implemented in your paper. If you have had any changes in phone/fax or e-mail addresses since your paper was submitted, please send us this new information.

PLEASE NOTE: Your corrections (modifications, deletions, additions, etc.) MUST be marked on the proof itself (either the hard copy proof, or the printed-out .PDF file) for return to the printer. We will no longer accept corrections indicated in a letter, summarized on a separate page, or inserted within the .pdf file itself.

FOURTH STEP:

You may choose one of the following methods to return your revised paper:

1. Regular mail, or via a courier service (please be advised that choosing to return your proof via regular mail from outside the United States can cause lengthy delays in the proof arriving here at the printing facility).
2. Fax
3. Scan the revised pages and attach to an E-mail.

Your revised paper needs to be faxed or mailed to:

IPC Print Services
Attn: Shannon Howell
501 Colonial Drive
St. Joseph, MI 49085
Fax number: 1-269-983-4064

If you have questions regarding your paper in general, you may email or telephone:

IPC Print Services
Attn: Shannon Howell
Email: showell@ipcjci.com
Phone: 1-269-983-7412, ext. 519